Guided wave sensitivity prediction for part and through thickness crack-like defects

Paul Fromme

Department of Mechanical Engineering, University College London, WC1E 7JE, UK
p.fromme@ucl.ac.uk

Short title: Guided wave scattering

Abstract

Guided waves allow for the efficient Structural Health Monitoring (SHM) of large structures using phased or distributed arrays of sensors. The sensitivity for specific defects can be improved by accounting for the angular scattering pattern. The scattering of the fundamental anti-symmetric guided wave mode (A_0 Lamb mode) at through-thickness and part-through crack-like defects was studied experimentally and from three-dimensional (3D) Finite Element (FE) simulations. Experimentally the scattered field around manufactured notches of different depths and lengths in an aluminum plate was measured using a laser interferometer. The scattered field was extracted by taking the complex difference in the frequency domain between a baseline measurement and measurements around the defect. Good agreement was found between measurements and 3D FE simulations and the amplitude and directionality pattern of the scattered field can be predicted accurately. The angular directionality pattern of the scattered field depending on the direction of the incident wave relative to the crack-like defect orientation, depth, and length relative to the wavelength were investigated. For short and part-thickness defects the main scattering effect is a reduction of the (forward) wave propagating past the defect with very limited back-scattered amplitude. Significant energy scattered back towards the incident wave direction was only found for perpendicular incidence on long and deep defects. Even for large defects almost no energy is scattered in certain directions from the defect, possibly complicating defect detection. Based on the predicted amplitude and angular dependency of the scattered guided waves, the sensitivity for defect detection using localized and distributed SHM sensor array systems can be quantified.

Keywords: A_0 Lamb wave, Guided Ultrasonic Waves, Scattering, Plate, Notch

1. INTRODUCTION

Guided ultrasonic waves (GUW) can propagate over long distances in structures that are thin in at least one dimension [1]. This offers an efficient method for the structural health monitoring (SHM) of large structures [2], e.g., for the detection of fatigue cracks in aircraft using guided wave arrays. Many investigations of guided wave SHM employ selective mode excitation of the fundamental modes (A_0, S_0) below the cut-off frequencies of the higher Lamb wave modes to achieve long propagation distances in plates and a simpler signal interpretation [3]. Localized phased array systems consist of an array of sensor elements at one location of the structure [4, 5] and allow for the detection of defects in a structure based on the analysis of back-scattered waves. Distributed guided wave array systems using sensor elements placed at a number of locations of the structure have been developed [6]. Taking the scattering directionality pattern of defects into account, e.g., using minimum variance imaging [7], defect detection and characterization capabilities have been shown to be improved. Crack-like defects show a directionality pattern of the scattered guided ultrasonic wave depending on the angle of the incident wave relative to the defect orientation and on the ratio of the defect length to wavelength [8].

Analytical solutions exist for the scattering of bulk ultrasonic waves at cracks and other obstacles [9] but are limited for guided waves [10]. The scattering at a circular hole was calculated analytically and compared to detailed experimental measurements for the fundamental anti-symmetric Lamb wave mode (A_0) [11] and fundamental symmetric Lamb wave mode (S_0) [12]. The scattering and mode conversion at part-thickness circular holes was studied analytically [13]. The practically relevant case of cracks at a circular hole was investigated using Finite Difference Modelling (FDM) [14], Finite Element Modelling (FEM) [15], and a hybrid FEM model [16], comparing and validating the resulting scattering patterns to experimental measurements. Good agreement for the local scattered amplitude field [14] and frequency spectra [16] was found for short cracks and notches relative to the hole diameter. Far-field scattering patterns for a long, through thickness notch emanating from a hole of varying diameter were validated experimentally for a range of excitation frequencies [15]. The scattering patterns of the A_0 mode at defects at a circular hole were investigated experimentally, evaluating the far field measured on radial lines using the Hankel transform [17]. Significant differences in the scattering patterns between a machined notch and fatigue crack emanating from the hole were found, depending on the ratio of the wavelength to defect length and direction. Similar methodology was also employed to compare the A_0 mode scattering patterns at impact damage and artificial delaminations in composite plates [18], and for the detection and monitoring of short fatigue cracks emanating from holes using higher order guided wave modes [19].

Hybrid approaches [20] and the use of orthogonality relations [21] were employed to investigate the scattering of guided ultrasonic waves at part-thickness defects and to reduce the computational effort required. Hybrid FEM models were also used to investigate the scattering of flexural waves at a crack [22]. The influence of length to incident wavelength was investigated using FEM for through thickness cracks and verified from experiments [23]. The angular scattering pattern for the SH_0 wave mode at cracks in plates was studied

[24]. Experimentally the scattering pattern around cracks was measured for the A_0 wave mode [25] and practical measurements to ascertain crack orientation and length have been proposed [26].

This contribution investigates the angular dependency and directionality pattern of the A_0 Lamb wave mode scattered at a crack-like defect (notch) in a plate, depending on the angle of the incident wave relative to the defect orientation and on the notch length relative to the wavelength. It is partially based on previous conference proceedings papers [8, 27-29], where the employed methodology and preliminary results were presented. The scattered wave fields predicted from Finite Element (FE) simulations and measured experimentally were compared and show good agreement for part-through and through thickness notches of different lengths. The obtained scattering characteristics for a systematic variation of the parameters are discussed with a view towards detection of crack-like defects using guided ultrasonic wave arrays for SHM.

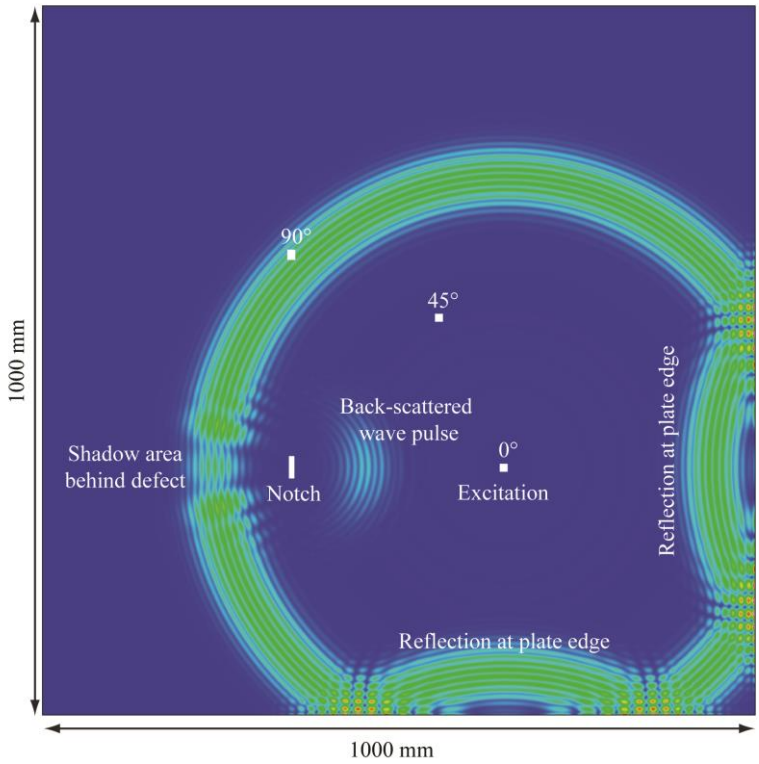

FIGURE 1. Time snapshot of FE plate simulation, top view; f = 100 kHz; λ = 19 mm; a = 20 mm; through thickness defect and excitation locations at 0°, 45°, and 90° shown; wave crest propagating radially outwards from 0° excitation, back-scattered wave at notch and lower amplitude behind defect visible.

2. FINITE ELEMENT SIMULATION AND PROCESSING

The propagation and scattering of the A_0 Lamb wave mode in plates was simulated using three-dimensional (3D) Finite Element (FE) models with linear brick elements (C3D8R, $\Delta x = \Delta y = 1$ mm, $\Delta z = 0.625$ mm) in ABAQUS Explicit. The model of a 5 mm thick aluminum plate (size: 1 m x 1 m) with a defect of varying length and depth was implemented (Fig. 1), similar to the model described in [8, 27]. The notch was modeled by removing one row of the brick elements to achieve the desired length and depth. This resulted in a notch with right angle corners and a width of 1 mm, matching the experimental

configuration described below reasonably well. The element size was not changed in the vicinity of the defect; therefore small errors might occur in the near field due to the description of the stress concentration using linear elements. Explicit time integration was used, and the element size and time step of 0.1 μs were chosen to adhere to the usual stability criteria [30].

Point excitation of the A_0 Lamb wave mode was introduced at chosen node locations 300 mm from the defect location, allowing for a variation of the incidence angle between 0° and 90° (range required due to symmetry of geometry), relative to the normal of the notch. An out-of-plane force was applied to the selected center (mid-plane) node to selectively excite the A_0 mode below the cut-off frequencies of the higher wave modes. The excitation pulse was set as a 5 cycle toneburst modulated by a Hanning window with a center frequency f of 100 kHz, giving a wavelength λ for the A_0 mode of 19 mm. The amplitude of the A_0 mode was monitored as the out-of-plane displacement at the center (mid-plane) node on points in a square area of 60 mm by 60 mm around the notch center. The time trace at each monitoring node was time gated to remove reflections from the plate edges.

Fast Fourier Transform (FFT) was used to extract the complex magnitude (amplitude and phase information) at the center frequency of 100 kHz for each monitoring node. This captures the combined wave field U_1 of the incident wave U_i and scattered wave U_s (Eq. 1), shown in Fig. 2a/b for a 0° incident wave. The typical scattering pattern with large amplitude at the free surface of the defect and forward scattering behind the defect can be seen. Along the incident direction (positive x axis) a periodically alternating high and low amplitude pattern due to the positive and negative interference of the incident wave U_i and back scattered wave U_s, according to their phase, can be observed.

$$U_1 = U_i + U_s \tag{1}$$

$$U_2 = U_i \tag{2}$$

$$A_s = |U_s| = |U_1 - U_2| \neq A_1 - A_2 = |U_i + U_s| - |U_i| \tag{3}$$

Additional simulations were run to capture the incident wave field U_i only (Fig. 2c), without a defect present (Eq. 2). Taking the difference between the complex magnitudes for each point with and without a defect (Eq. 3), the amplitude of the wave scattered at the notch (Fig. 2d) can be isolated [28]. All amplitudes were normalized relative to the amplitude of the incident wave at the center location without a defect present.

It should be noted that the phase information contained in the complex magnitude is necessary for this subtraction, as a simple subtraction of the measured amplitudes with and without a defect does not give the amplitude of the scattered wave only (Eq. 3). For the employed narrowband pulses, the equivalent analysis in the time domain would be to take the difference for the time traces with and without defect and to record the maximum amplitude of the difference signal envelope. This could be a practical approach (e.g. when time gating is difficult), and leads to similar scattering patterns but with slightly lower amplitude, as effectively the analysis averages over the frequency content of the narrowband pulse.

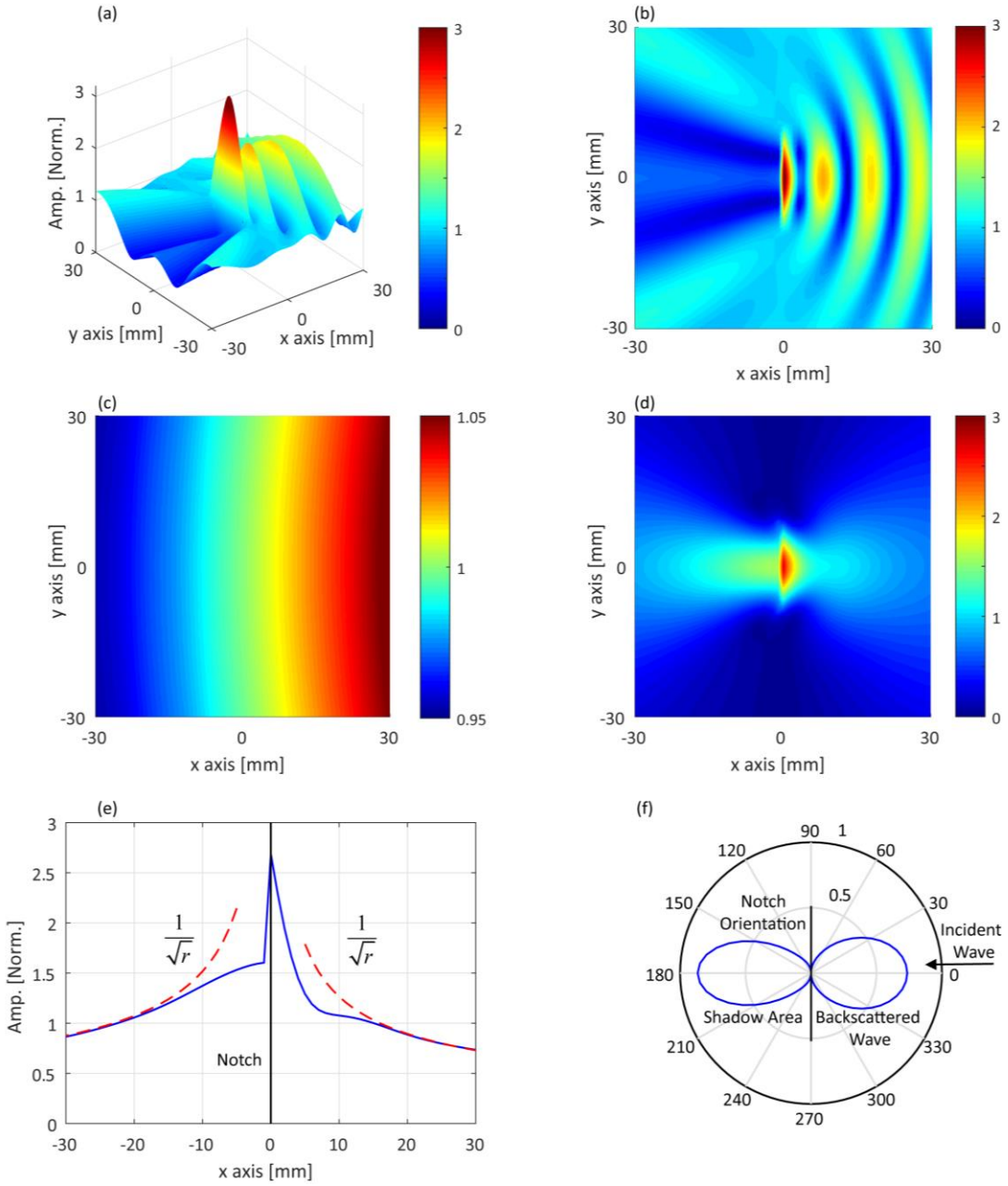

FIGURE 2. Normalized amplitude of scattered guided wave field (A_0 mode) at through thickness notch; f = 100 kHz; λ = 19 mm; a = 20 mm: a) angular view of combined field; b) top view of combined field; c) incident wave field only; d) scattered wave field only; e) scattered amplitude (blue, solid) along x axis (perpendicular to defect) and radial dependency (red, dashed); f) polar plot of normalized amplitude (monitored at 30 mm radius).

The scattered wave field (Fig. 2d) shows the expected behavior for a wave incident perpendicular on a long through-thickness defect (length a = 20 mm similar to wavelength λ = 19 mm), with a significant forward scattering behind the defect (negative x axis) and back scattered wave (positive x axis). Evaluating the scattered field on a radial line (x axis) more than a wavelength (19 mm) away from the defect (Fig. 2e), the amplitude shows a decrease proportional to one over the square root of the distance, as would be expected for a point source of the guided wave mode on a plate. Therefore, the amplitude of the scattered wave was extracted on a radius of 30 mm by interpolating between monitoring nodes to obtain an amplitude value every 5 degree. Shown in Fig. 2f is the polar plot of the

normalized amplitude of the scattered A_0 mode, from which the forward scattering behind the defect and the back scattered wave can be clearly identified. Using the radial square root dependency relative to the monitoring radius of 30 mm, the amplitude of the scattered wave at any location in the plate can be predicted. Simulations were run to match the experimental configurations (chapter 3) and for variations of the notch length and depth as well as the angle of the incident wave relative to the defect orientation in 5° steps.

3. EXPERIMENTS

The scattered wave field around 20 mm and 6 mm long notches was measured on a large, 5 mm thick aluminum plate (size: 1.5 m x 1 m) [27, 29]. The 20 mm long notch (width: 1 mm) was milled in four steps to give a varying depth of 1.25 mm (1/4 thickness), 2.5 mm (1/2 thickness), 3.75 mm (3/4 thickness) and through thickness. The notch had straight edges but rounded corners due to the milling tool (diameter 1 mm) and a flat bottom for the part-through depths. The milling for the 20 mm long notch was performed in the workshop, requiring the re-positioning of the plate after each milling step and reducing the repeatability of the phase measurement. This leads to a noise level of about 5% of the amplitude of the incident wave when taking the difference between complex magnitudes to evaluate the scattered field. The 6 mm long notch (width: 1 mm) was manufactured in situ with depths of 2.5 mm (1/2 thickness) and through thickness, using hand-held tools. This resulted in slightly uneven edges and depth of the notch, but did not require re-positioning of the plate and reduced the noise level to about 3%.

Three excitation transducers were placed 300 mm away from the center of the notch location to give angles of the incident wave of 0°, 45° and 90° relative to the normal of the notch (Fig. 3). The transducers consist of a PZT disc (Ferroperm Pz27, diameter 5 mm, thickness 2 mm) and a brass backing mass (height 6 mm) and were permanently bonded to the plate using two-component epoxy glue. The transducers act in good approximation as point sources for the excitation of the first antisymmetric Lamb wave mode A_0. The excitation signal was a 5 cycle toneburst with a center frequency of 100 kHz modulated by a Hanning window. The signal was generated in a programmable function generator and amplified using a power amplifier (200 Vpp). The velocity of the out-of-plane displacement was measured using a laser interferometer every 5 degrees on a circle around the notch with a radius of 30 mm. The full time traces of the measured signals were bandpass filtered (75 kHz – 125 kHz) and averaged (20 averages) in a digital oscilloscope before being transferred to the measurement PC [29, 8]. Similar to the FE simulations, an initial measurement was done for each excitation transducer before the milling of the notch to capture the incident wave field, and then for each notch depth. The measured time traces were time gated and the amplitude and phase (complex magnitude) at 100 kHz determined using FFT. Amplitudes for each incident direction were normalized relative to the amplitude of the incident wave measured at the defect center location before the notch was manufactured.

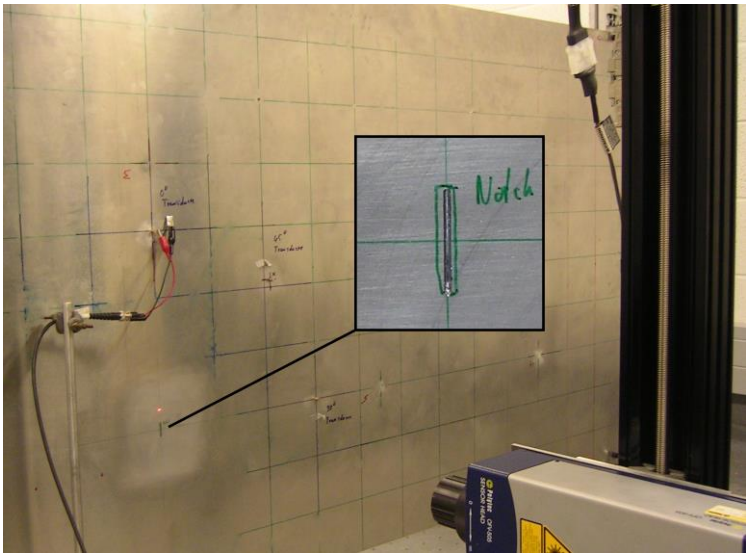

FIGURE 3. View of experimental setup: aluminum plate (size: 1.5 m x 1 m) with 20 mm notch (zoom), 3 excitation transducers at 0°, 45°, and 90°, 300 mm from notch, and laser interferometer.

4. COMPARISON OF EXPERIMENTAL AND SIMULATION SCATTERING PATTERNS

In order to verify the FE predictions, simulation and experimental results were compared for 20 mm and 6 mm long notches partially and fully through the thickness of the 5 mm thick aluminum plate. For each case, the summed square of the difference in amplitude between experimental and simulation results was normalized by the summed squared amplitude of the simulation curve and is presented as a percentage difference to quantify the agreement. It should be noted that this measure includes both a contribution from experimental noise and systematic differences, e.g., scattering lobes at different angles or amplitudes.

For the incident wave perpendicular to the 20 mm long notch (0° incidence angle) generally good agreement of the angular amplitude patterns between FE predictions and experimental results can be seen in Fig. 4 for all notch depths (¼, ½, ¾, through) [27]. For a shallow defect ¼ of the plate thickness two lobes of the scattered wave perpendicular to the defect orientation can be seen with maximum amplitude of less than 20% of the amplitude of the incident wave. As mentioned above, the noise level for the complex magnitude difference calculated from experimental results is about 5%, which is evident in Fig. 4a, and leads to a percentage difference of 10% between simulation and experimental results. For increasing depth of the defect initially an increase of the forward scattering behind the defect can be observed for a ½ thickness notch (5% difference with slightly lower measured forward scattering amplitude), as the path of the incident wave is blocked and mode conversion to the S_0 and SH_0 modes occurs. For a ¾ depth defect the forward scattering increases, with only very limited energy propagating past the defect. Significant back-scattered amplitude is only observed for a notch ¾ through the plate thickness (about 30%), increasing to 70% for a through thickness defect. For the ¾ and through thickness defects very good agreement between measurements and FE simulations was found, with a percentage difference of less than 1% for both cases.

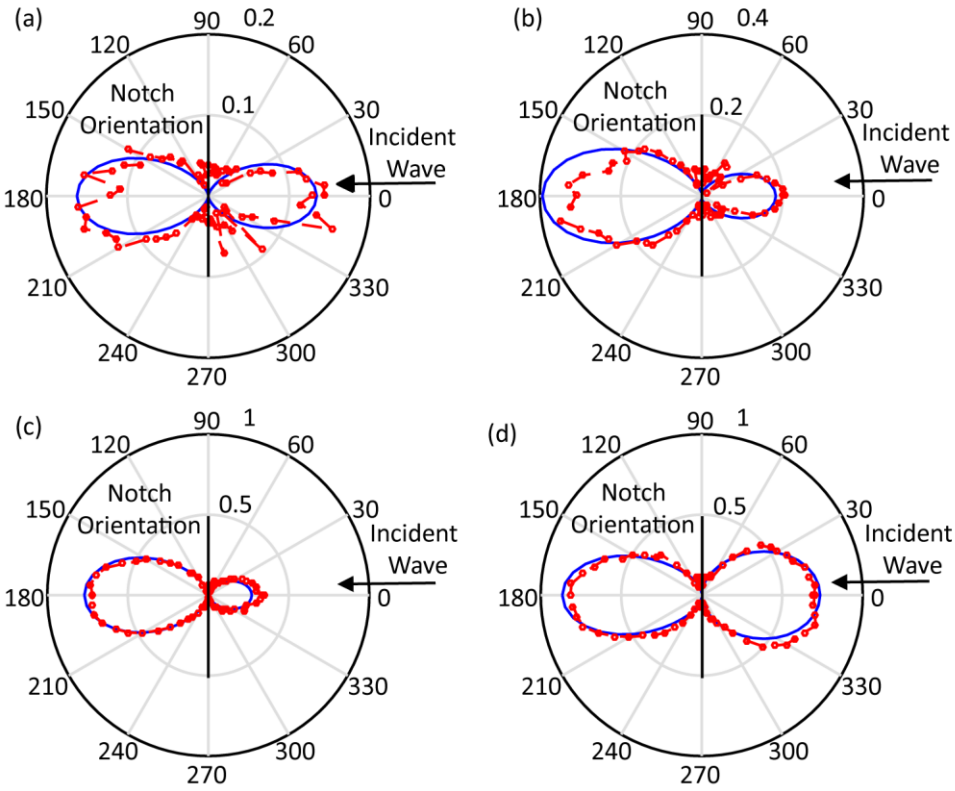

FIGURE 4. Polar plot of normalized amplitude of A_0 mode scattered at notch (monitored at 30 mm radius); orientation 90°-270°; incident wave from 0°; f = 100 kHz; λ = 19 mm; a = 20 mm; experiment (red, dots), simulation (blue, solid): a) ¼ thickness; b) ½ thickness; c) ¾ thickness; d) through thickness.

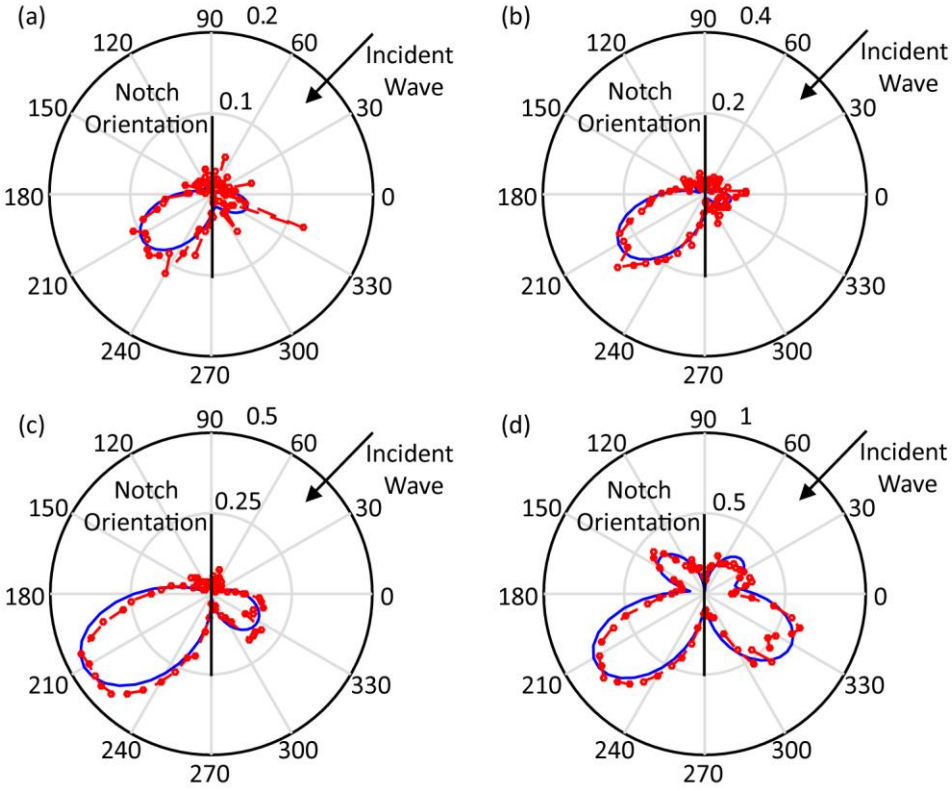

FIGURE 5 Polar plot of normalized amplitude of A_0 mode scattered at notch (monitored at 30 mm radius); orientation 90°-270°; incident wave from 45°; f = 100 kHz; λ = 19 mm; a = 20 mm; experiment (red, dots), simulation (blue, solid): a) ¼ thickness; b) ½ thickness; c) ¾ thickness; d) through thickness.

For the incident wave at a 45° angle relative to the 20 mm long defect again good agreement was found between experiments and the FE calculations (Fig. 5) [27]. For shallow defects of ¼ and ½ plate thickness mostly forward scattering behind the notch in the direction of wave propagation was observed (Fig. 5a/b), with a significant reflected wave only present for a deep defect (Fig. 5c/d). Due to the lower scattered amplitudes compared to the 0° case, the relative differences are slightly higher with 15% for the ¼ thickness case and 7% for the half thickness case, mostly due to measurement noise. For the ¾ and through thickness cases, good agreement with 3% difference was found, with a small, systematic difference of the angle of the main forward scattered lobe between experiments and FE simulations. The main reflection for the 20 mm long notch is in the 325° direction, with only low amplitude scattered back in the direction of the incident wave (45°). From an evaluation of the predicted angular scattering patterns it was found that the reflection angle approaches the specular angle of 315° for longer defects (28 mm and above, not shown), so this is likely due to the defect length being similar to the wavelength and not perfectly fulfilling the conditions for a reflection at an infinite boundary. It should be noted that for this case, where the wave is incident on the defect at a large angle of 45°, the amplitude of all scattered wave lobes, while significant and clearly observable, are lower than for the perpendicular incidence case discussed above. For both incident wave directions, almost no energy is scattered along the defect orientation (90° or 270°). Previously, the scattering patterns had also been compared to FE simulations for a crack (zero width) [29], where in general similar angular scattering patterns, but, depending on the geometry, some differences of the amplitudes were observed.

For the incident wave propagating along the defect orientation (90° angle), only a small scattered wave is expected for a ½ thickness notch of about 5% amplitude of the incident wave and thus difficult to detect the defect, even from a local laser measurement (Fig. 6a, 39% difference between simulation and experiment). For the through thickness defect scattered amplitude of about 8% of the incident wave amplitude was predicted and could be measured for the 90° incidence angle with a difference of 14% to the simulation results, as it was larger than the noise level of around 5% of the amplitude of the incident wave (Fig. 6b).

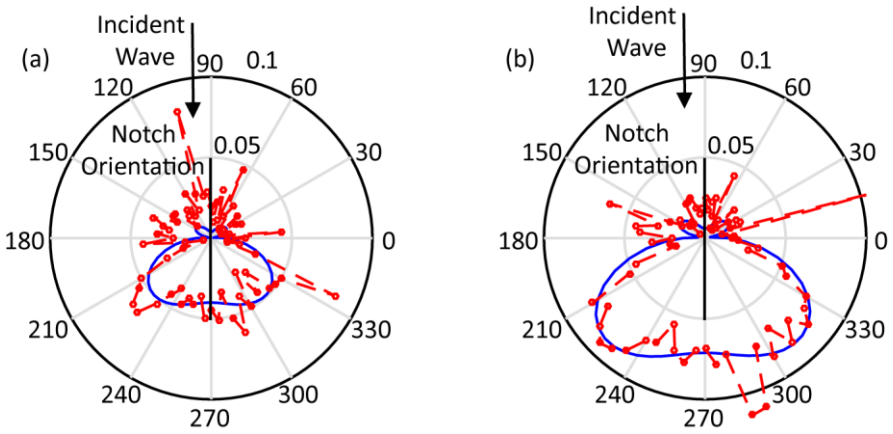

FIGURE 6 Polar plot of normalized amplitude of A_0 mode scattered at notch (monitored at 30 mm radius); orientation 90°-270°; incident wave from 90°; f = 100 kHz; λ = 19 mm; a = 20 mm; experiment (red, dots), simulation (blue, solid): a) ½ thickness; b) through thickness.

For the 6 mm long defect, the FE simulations predicted a maximum amplitude of less than 5% for 90° incidence for any depth and ¼ thickness for any incident direction. Due to the noise levels inherent in the measurements, it would not be possible to discern these from measurements. For the 0° incident wave mostly forward scattering with an amplitude reduction behind the defect was predicted. Reasonable agreement with the measured scattered fields for ½ thickness (Fig. 7a, 41% difference), and through thickness (Fig. 7b, 6% difference) can be seen, with increasing maximum scattered amplitude. However, it must be noted that the noise level is rather high compared to the scattered wave amplitude, limiting the accuracy of the validation, especially for the ½ thickness case. Figure 7c/d show the case for 45° incidence on the 6 mm long, ½ thickness and through thickness defect. Lower amplitude than for the 0° incident wave can be seen, with the angular scattering pattern for both cases mostly consisting of forward scattering behind the defect. For the half thickness case, a difference of 57% between experimental and simulations results was found, reducing to 19% for the through thickness case, again limiting the accuracy of the validation.

Within the limitations of the measurement noise, overall good agreement of the predicted scattering patterns from the FE simulations with the measurements was found, allowing the investigation of the influence of length, depth, and incident angle for a wider range of values from FE simulations.

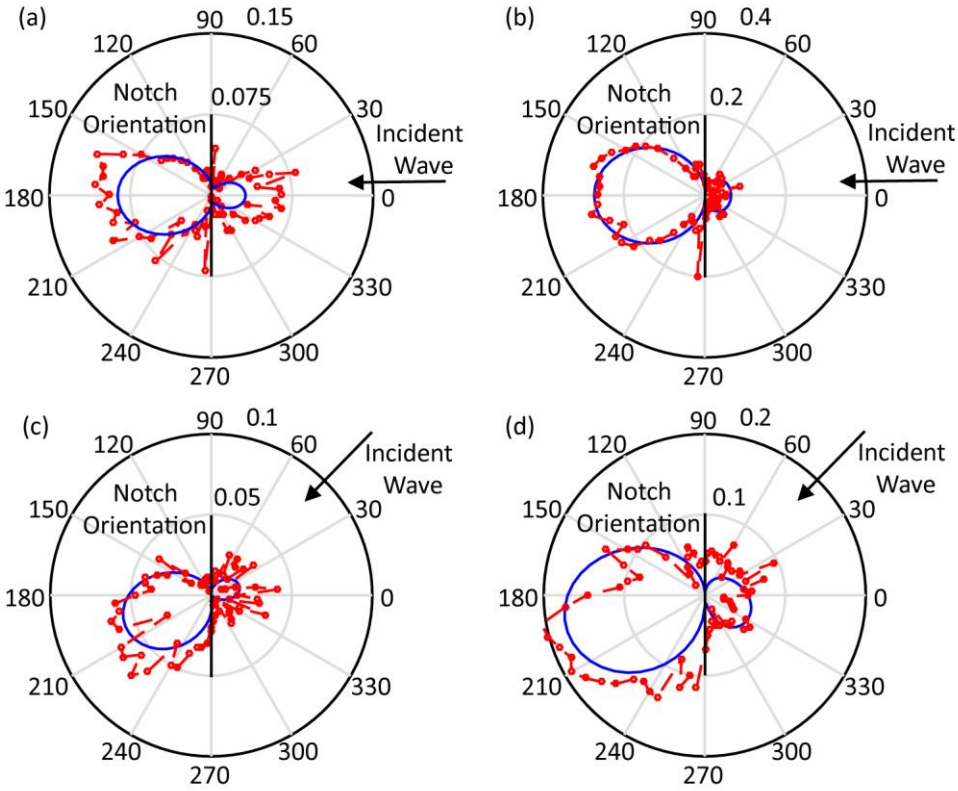

FIGURE 7 Polar plot of normalized amplitude of A_0 mode scattered at notch (monitored at 30 mm radius); orientation 90°-270°; f = 100 kHz; λ = 19 mm; a = 6 mm; experiment (red, dots), simulation (blue, solid): a) ½ thickness; incident wave from 0° b) through thickness; incident wave from 0° c) ½ thickness; incident wave from 45°; d) through thickness; incident wave from 45°.

5. ANALYSIS OF DIRECTIONALITY SCATTERN PATTERNS

5.1. Defect depth

The influence of the defect depth on the scattered wave amplitude and angular pattern was evaluated in more detail from FE simulations for defect lengths of 6 mm (λ/3), 10 mm (λ/2) and 20 mm (λ). Figure 8 shows the maximum scattered amplitude for incident directions from 0° and 45°. For all cases considered, the maximum amplitude was observed in the forward direction, with the back-scattered amplitude lower, especially for short and shallow defects. For a short defect (6 mm), mostly a blocking of the incident wave occurs, with forward scattering behind the defect (as seen in the angular scattering patterns in Fig. 7). For shallow defects, the maximum amplitude of the scattered wave is low (less than 10% of incident wave amplitude) and increases almost linearly with defect depth (Fig. 8a/b). The scattered wave amplitude increases markedly for the through thickness defect and could be measured accurately for both incident wave directions (Fig. 7b/d).

For the 10 mm long defect (λ/2) again the maximum scattered wave amplitude is rather low for part thickness defects (Fig. 8c/d), approximately twice the magnitude as for the 6 mm long defect. The amplitude increases markedly for the defect through the plate thickness and a back-scattered wave lobe perpendicular to the defect orientation was found for both incident wave directions (Fig. 9a/c).

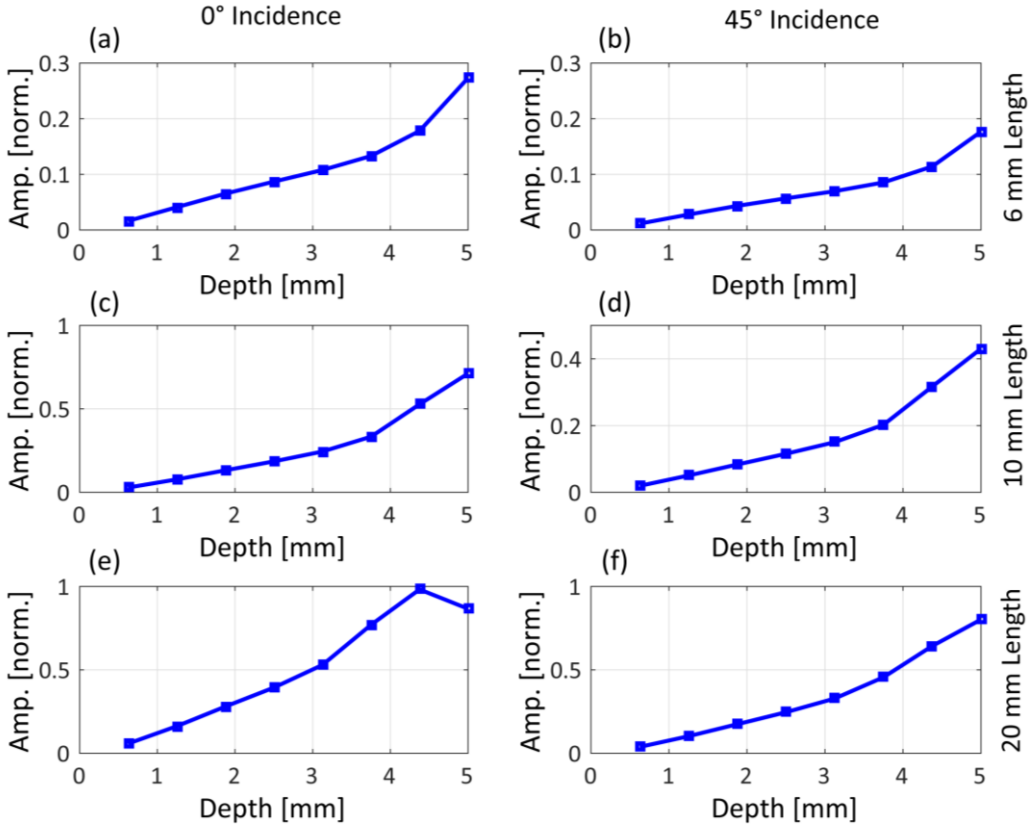

FIGURE 8. Maximum normalized amplitude of A_0 mode scattered at defect for variation depth; a) a = 6 mm, incident wave 0°; b) a = 6 mm, incident wave 45°; c) a = 10 mm, incident wave 0°; d) a = 10 mm, incident wave 45°; e) a = 20 mm, incident wave 0°; f) a = 20 mm, incident wave 45°.

When the defect length approximates the wavelength (a = 20 mm), the scattered wave amplitude increases significantly (Fig. 8e/f). For the 0° incident wave direction, a back-scattered wave develops for part-thickness defects and increases in magnitude to close to (but still lower) the amplitude of the forward scattered wave lobe for through thickness defects (Fig. 4). The highest scattered amplitude was found for a notch depth of 4.25 mm rather than through the thickness (Fig. 8e). For the 45° incidence case, a specular scattering pattern with significant amplitude only develops when the defect depth approaches the plate thickness (Fig. 5).

In summary, the scattered wave amplitude is small for short and shallow defects and only approached the incident wave amplitude for through thickness defects longer than half the wavelength. The largest scattering contribution for all considered cases is a forward scattering with the defect blocking the incident wave energy. This indicates that the detection of part-thickness defects is difficult, especially if it relies on the measurement of a back-scattered wave as for the phased array SHM approach [4].

5.2. Defect length

The influence of the defect length relative to the wavelength (λ = 19 mm) was investigated for through-thickness and ½ thickness defects oriented perpendicular (0°) and at an angle (45°) to the direction of the incident wave [29]. Figures 9 and 10 show respectively the angular scattering patterns and maximum scattered amplitude for through thickness (Fig. 9) and half thickness (Fig. 10) notches with the incident wave perpendicular (0°) and from the 45° direction. For short, through thickness defects (up to about 6 mm, $\lambda/3$), a low amplitude forward scattering behind the defect was found, as it blocks part of the wave energy (Fig. 9a/c). When the defect length reaches approximately half of the wavelength (10 mm), the back-scattered lobe increases significantly in amplitude. Interestingly, for this defect length both for 0° and 45° incident wave direction, the angular scattering patterns remains mostly symmetric to the 0° direction, i.e., the waves are scattered mostly perpendicular to the defect orientation (Fig. 9a/c). The maximum amplitude of the scattered wave field increases up to 10 mm defect length, but then plateaus for both incident wave directions (Fig. 9b/d). This can be interpreted as more of the wave energy being back-scattered, while the forward scattering does not increase significantly. For defects of similar length to the wavelength (λ = 19 mm), a strong back-scattered wave for the 0° incidence direction can be observed and an approximately specular scattering pattern with 2 large and 2 smaller lobes for the 45° incidence case. The maximum amplitude of the scattered wave continues to increase with defect length, but with steps rather than linearly. The maximum amplitude of the scattered wave always occurs in the forward direction and can be larger than the amplitude of the incident wave, as energy is directed in specific directions rather than scattered uniformly. Similar scattering patterns with lobes of the scattered field corresponding to the angle between the incident wave and the defect orientation can be observed for other angles of the incident wave when the defect length is comparable to the wavelength (λ = 19 mm). It can be seen that the directionality pattern depends on the ratio between the wavelength and the defect size [8] and that along the orientation of the defect, almost no energy is scattered.

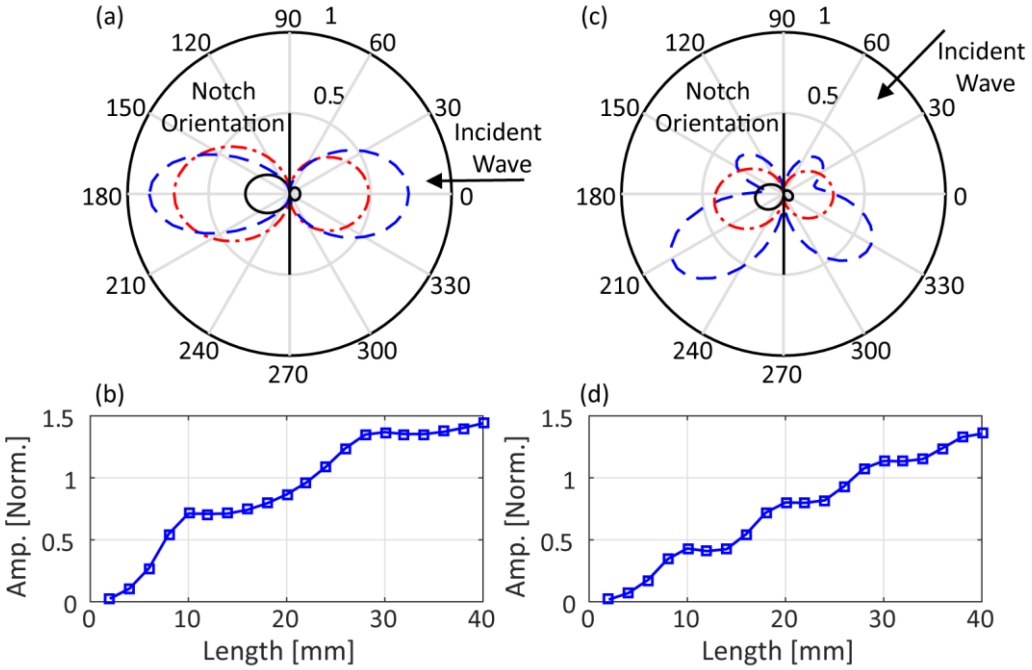

FIGURE 9. Normalized amplitude of A_0 mode scattered at defect; through thickness; a) polar plot: a = 6 mm (black, solid), a = 10 mm (red, dash-dotted), a = 20 mm (blue, dashed), incident wave from 0°; b) maximum amplitude for variation length, incident wave from 0°; c) polar plot: a = 6 mm (black, solid), a = 10 mm (red, dash-dotted), a = 20 mm (blue, dashed), incident wave from 45°; d) maximum amplitude for variation length, incident wave from 45°.

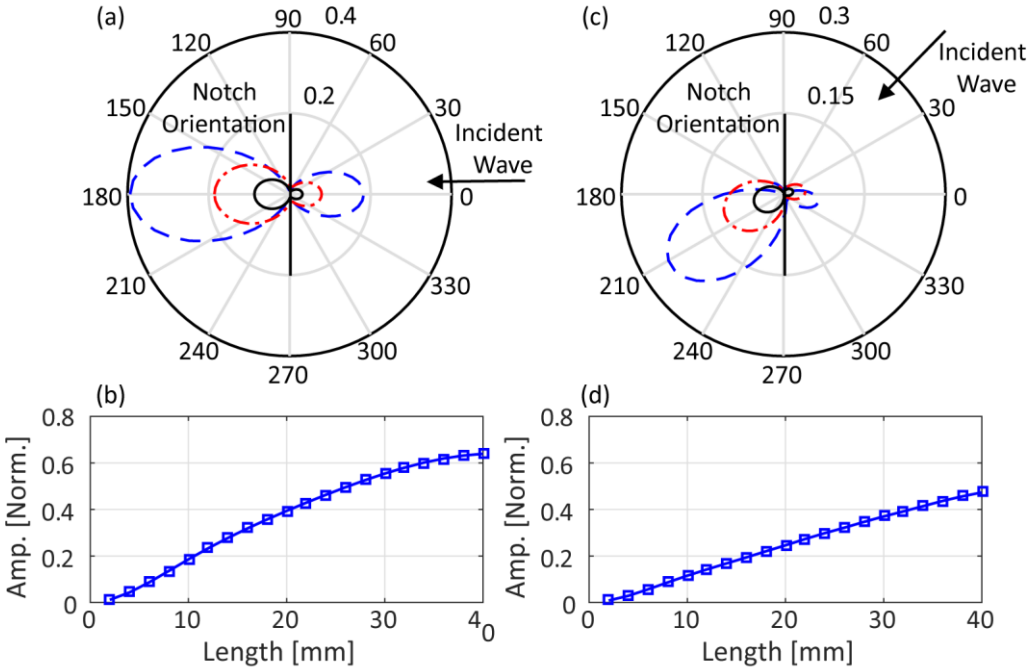

FIGURE 10. Normalized amplitude of A_0 mode scattered at defect; ½ thickness; a) polar plot: a = 6 mm (black, solid), a = 10 mm (red, dash-dotted), a = 20 mm (blue, dashed), incident wave from 0°; b) maximum amplitude for variation length, incident wave from 0°; c) polar plot: a = 6 mm (black, solid), a = 10 mm (red, dash-dotted), a = 20 mm (blue, dashed), incident wave from 45°; d) maximum amplitude for variation length, incident wave from 45°.

For the ½ thickness case (Fig. 10), the maximum amplitude of the scattered wave field increases more smoothly with defect length (Fig. 10b/d), but is significantly lower than for through thickness defects. For 0° incidence, a significant back-scattered wave can only be

observed when the defect length approaches the wavelength, with the main effect a partial blocking of the forward direction (Fig. 10a). For the incident wave from the 45° direction, the angular variation of the scattered field is less pronounced than for the through thickness defect (Fig. 10c), mostly only showing forward scattering with a reduction of the amplitude. For all cases, the backscattered amplitude is lower than the forward scattering. Even for a 20 mm long, ½ thickness notch rather low backscattered or specular reflected wave amplitude is observed, making detection based on observation of a backscattered wave difficult.

5.3. Incident Wave Direction

From the above results, a significant influence of the angle of the incident wave relative to the defect orientation on the angular scattering pattern and amplitude was observed [8, 28]. The maximum scattered wave amplitude was systematically studied for variation of the incidence angle in 5° steps for through and part thickness defects of 6mm, 10 mm, and 20 mm lengths (Fig. 11). For a short, through thickness defect (6 mm, λ/3) the angular scattering pattern is dominated by forward scattering behind the defect for all incidence angles but almost no back-scattered wave (not shown). The maximum scattered amplitude decreases with higher incident wave angles from 27% to 2% (Fig. 11a). For a 10 mm long through thickness defect (λ/2) the maximum forward scattered amplitude for perpendicular incidence (0°) is much higher (71%), but then reduces to similar values as for the shorter defect (4%) for the incident wave propagating along the defect (90°). For incidence angles up to about 60° a second, back-scattered lobe was evident, but with lower amplitude (as shown in Fig. 9a/c).

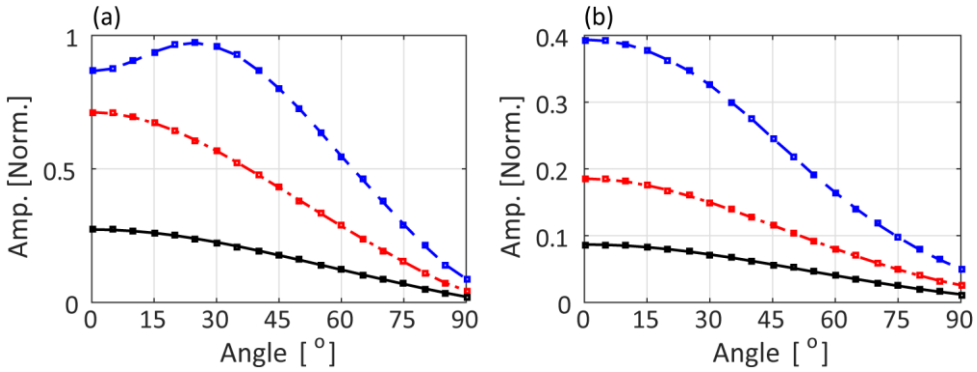

FIGURE 11. Normalized amplitude of A_0 mode scattered for variation of direction incident wave to defect; (a) through thickness; (b) ½ thickness; a = 6 mm (black, solid); a = 10 mm (red, dash-dotted); a = 20 mm (blue, dashed).

For a defect length of 20 mm (λ), contrary to what was originally expected, the maximum amplitude of the scattered field was for an incident angle of 25° rather than 0° (Fig. 11a). The maximum scattered amplitude varies between 80% and 100% for incidence angles up to 45° and multiple lobes of the angular scattering pattern can be observed up to about 60° incidence angle. For the incident wave along the defect orientation, again the scattered wave amplitude drops to about 8%, as confirmed from experiments (Fig. 6b).

The maximum scattered amplitude for part-thickness (½ thickness) defects is much lower (Fig. 11b), reaching 39% for 20 mm length, 19% for 10 mm length, and 9% for 6 mm length for perpendicular incidence (0°). The scattered amplitude drops for higher incident wave

directions to 5% or less for the 90° incidence case. The highest amplitude is in the forward scattered direction for all defect lengths, with a back-scattered wave only visible for perpendicular incidence on longer part-thickness defects (not shown).

5.4. Implications of scattered amplitude patterns on SHM defect detection

Experiments and FE simulations show the expected general trend that the maximum scattered wave amplitude increases with defect length and depth. Part-thickness defects have significantly lower scattered amplitude than through thickness defects of the same length, indicating limitations for the detection of shallow fatigue cracks before they have grown through the specimen thickness. The increase in amplitude with defect size is not always linear, and especially for the defect length approaching the wavelength, complex angular patterns develop with wave energy scattered in specific directions. For all considered cases, the forward scattering had higher amplitude than the back-scattered wave, making defect detection based on pulse-echo configurations (phased array) potentially less sensitive than pitch-catch concepts (distributed sensors). For most cases, the scattered wave amplitude increases for perpendicular incidence. Interestingly, this is not always the case (see e.g. Fig. 11a), and care must be taken to incorporate this for defect characterization.

For shallow and short defects the main influence is a forward scattering with the defect reducing the wave energy behind its location. Only rather limited energy is reflected back towards the excitation transducer location. This could significantly influence the ability to detect a defect from pulse-echo type measurements using a localized, phased array of guided wave transducers [4], which typically relies on the signal scattered back to the sensor location. For sparse arrays, good detection sensitivity has been reported in literature for defects located within the area covered by the distributed sensors [31], i.e., having sensitivity to changes in signals on the forward scattered wave path.

For through-thickness defects, the observed scattering patterns show significant similarities to those obtained by Liu et at [15] for the incremental scattering of a long notch emanating from a circular hole. For perpendicular and 45° incidence directions, the angular patterns have similar lobe structures when the wavelength is comparable to the combined hole and notch dimensions, indicating that when the hole diameter is small compared to the notch length, the guided wave scattering is dominated by the notch. However, for the 90° case (incident wave along notch orientation), Liu et al [15] found significant differences depending on whether the notch is located above or below the hole, and such cases would not be accurately presented by the results in this contribution.

The amplitude of the scattered wave shows a strong angular dependency and along the defect orientation direction almost no energy is scattered. This can pose a problem for SHM applications as for given transducer locations on a structure, there exist possible defect (crack) positions and orientations, where even for a severe defect no signal from the defect would be detected due to the scattering directionality pattern of the defect. This can help to explain the improved performance by advanced signal processing algorithms such as Minimum Variance Imaging [7], which take the expected damage scattering pattern into account. For cases where the stress field and thus likely location and orientation of fatigue cracks is known, sensor placement can be optimized to achieve (as much as possible)

perpendicular incidence and/or measurement in the forward path. Imaging using multipath [31] or edge-reflected [32] guided waves has been developed recently to use the additional information contained in the signals and shown to improve defect localization.

6. CONCLUSIONS

The scattering of the A_0 Lamb wave mode (fundamental anti-symmetric guided wave mode) at part-through and through thickness defects in an aluminum plate has been investigated experimentally and from 3D FE simulations of the wave propagation and scattering. Good agreement was found between the FE predicted and experimentally measured scattered field directivity patterns and amplitudes. This allows for the further investigation of the influence of relative defect size and depth, wavelength, plate thickness, and incidence angle from FE simulations only. For waves incident on the defect either perpendicular or at a not too large angle, a significant forward scattering could be observed for part-through thickness defects, while the amplitude of reflected wave lobes increased significantly only for deep or through thickness defects. For all considered cases the amplitude of the forward scattered wave was larger than the backscattered amplitude, making defect detection using arrays of distributed sensors better suited, especially for the detection of short and shallow defects. For incident waves propagating along the orientation of the defect, only for a through thickness notch a measurable scattered wave was observed. For all investigated cases of incidence angle and defect size it was found that in certain directions there is only very little scattered wave energy. These findings should be taken into account when developing permanently attached guided wave array systems for SHM, as the sensitivity for defect detection will depend strongly on the chosen geometric configuration in relation to the possible defect locations. Based on the investigation presented in this contribution, the sensitivity for the detection of defects at likely locations and orientations can be quantified and predicted. For different choices of wave mode or excitation frequency (and thus wavelength relative to the plate thickness), different scattering patterns would be expected and should be investigated.

References

[1] J. Li and J.L. Rose, Implementing guided wave mode control by use of a phased transducer array, IEEE Trans. Ultrason. Ferroelectr. Freq. Control 48, 761-768 (2001). https://doi.org/10.1109/58.920708

[2] H. Cho and C.J. Lissenden, Structural health monitoring of fatigue crack growth in plate structures with ultrasonic guided waves, Struct. Health Monit. 11, 393-404 (2012). https://doi.org/10.1177/1475921711430439

[3] D.N.Alleyne and P. Cawley, The interaction of Lamb waves with defects, IEEE Trans. Ultrason. Ferroelec. Freq. Cont. 39, 381-397 (1992). https://doi.org/10.1109/58.143172

[4] P. Fromme, P.D. Wilcox, M.J.S. Lowe and P. Cawley, On the development and testing of a guided ultrasonic wave array for structural integrity monitoring, IEEE Trans. Ultrason. Ferroelectr. Freq. Control 53, 777-785 (2006). https://doi.org/10.1109/TUFFC.2006.1621505

[5] L. Yu and V. Giurgiutiu, In situ 2-D piezoelectric wafer active sensors arrays for guided wave damage detection, Ultrasonics 48, 117-134 (2008). https://doi.org/10.1016/j.ultras.2007.10.008
[6] A.J. Croxford, P.D. Wilcox, B.W. Drinkwater and G. Konstantinidis, Strategies for guided-wave structural health monitoring, Proc. Roy. Soc. A 463, 2961-2981 (2007). https://doi.org/10.1098/rspa.2007.0048
[7] J.S. Hall, P. Fromme, and J.E. Michaels, Guided Wave Damage Characterization via Minimum Variance Imaging with a Distributed Array of Ultrasonic Sensors, J. Nondestruct. Eval. 33, 299-308 (2014). https://doi.org/10.1007/s10921-013-0212-x
[8] P. Fromme and C. Rouge, Directivity of guided ultrasonic wave scattering at notches and cracks, J. Phys. Conf. Ser. 269, 012018 (2011). https://doi.org/10.1088/1742-6596/269/1/012018
[9] D.A. Mendelsohn, J.D. Achenbach, and L.M. Keer, Scattering of elastic waves by a surface-breaking crack, Wave Motion 2, 277-292 (1980). https://doi.org/10.1016/0165-2125(80)90008-6
[10] G.C. Sih and J.F. Loeber, Flexural waves scattering at a through crack in an elastic plate, Engineering Fracture Mechanics 1, 369-378 (1968). https://doi.org/10.1016/0013-7944(68)90009-X
[11] P. Fromme and M.B. Sayir, Measurement of the scattering of a Lamb wave by a through hole in a plate, J. Acoust. Soc. Am. 111, 1165-1170 (2002). https://doi.org/10.1121/1.1448338
[12] J.C.P. McKeon and M.K. Hinders, Lamb wave scattering from a through hole, J. Sound Vib. 224, 843-862 (1999). https://doi.org/10.1006/jsvi.1999.2164
[13] F.B. Cegla, A. Rohde, and M. Veidt, Analytical prediction and experimental measurement for mode conversion and scattering of plate waves at non-symmetric circular blind holes in isotropic plates, Wave Motion 45(3), 162-177 (2008). https://doi.org/10.1016/j.wavemoti.2007.05.005
[14] P. Fromme and M.B. Sayir, Detection of cracks at rivet holes using guided waves, Ultrasonics 40, 199-203 (2002). https://doi.org/10.1016/S0041-624X(02)00137-3
[15] H. Liu, X. Chen, J.E. Michaels, T.E. Michaels, and C. He, Incremental scattering of the A0 Lamb wave mode from a notch emanating from a through-hole, Ultrasonics 91, 220-230 (2019). https://doi.org/10.1016/j.ultras.2018.08.004
[16] Z.S. Chang and A. Mal, Scattering of Lamb waves from a rivet hole with edge cracks, Mech. Mater. 31, 197-204 (1999). https://doi.org/10.1016/S0167-6636(98)00060-X
[17] N. Quaegebeur, N. Bouslama, M. Bilodeau, R. Guitel, P. Masson, A. Maslouhi, and P. Micheau, Guided wave scattering by geometrical change or damage: Application to characterization of fatigue crack and machined notch, Ultrasonics 73, 187-195 (2017). https://doi.org/10.1016/j.ultras.2016.09.014
[18] M.H. Sherafat, N. Quaegebeur, p. Hubert, L. Lessard, and P. Masson, Experimental model of impact damage of guided wave-based inspection of composites, ASME J Nondestruct. Eval. 1, 040801 (2018). https://doi.org/10.1115/1.4040719
[19] C. Travaglini, C. Bescond, M. Viens, and P. Belanger, Feasibility of high frequency guided wave crack monitoring, Struct. Health Moni. 16, 418-427 (2017). https://doi.org/10.1177/1475921716673567

[20] Y. Shen and V. Giurgiutiu, Combined analytical FEM approach for efficient simulation of Lamb wave damage detection, Ultrasonics 69, 116–128 (2016). https://doi.org/10.1016/j.ultras.2016.03.019
[21] L. Moreau and M. Castaings, The use of an orthogonality relation for reducing the size of finite element models for 3D guided waves scattering problems, Ultrasonics 48, 357–366 (2008). https://doi.org/10.1016/j.ultras.2008.01.005
[22] R. Paskaramoorthy, A.H. Shah, and S.K. Datta, Scattering of flexural waves by a crack in a plate, Eng. Fract. Mech. 33, 589-598 (1989). https://doi.org/10.1016/0013-7944(89)90042-8
[23] Y. Lu, L. Ye, Z. Su, and C. Yang, Quantitative assessment of through-thickness crack size based on Lamb wave scattering in aluminium plates, NDT & E Int. 41, 59-68 (2008). https://doi.org/10.1016/j.ndteint.2007.07.003
[24] P. Rajagopal and M.J.S. Lowe, Angular influence on the scattering of fundamental shear horizontal guided waves by a through-thickness crack in an isotropic plate. J. Acoust. Soc. Am. 124, 2021-2030 (2008). https://doi.org/10.1121/1.2968697
[25] X. Chen, J.E. Michaels, and T.E. Michaels, A methodology for estimating guided wave scattering patterns from sparse transducer array measurements, IEEE Trans. Ultrason., Ferroelectr. Freq. Control 62, 208–219 (2015). https://doi.org/10.1109/TUFFC.2014.006747
[26] P.S. Tua, S.T. Quek, and Q. Wang, Detection of cracks in plates using piezo-actuated Lamb waves, Smart Mater. Struct. 13(4), 643-660 (2004). https://doi.org/10.1088/0964-1726/13/4/002
[27] P. Fromme, Directionality of the scattering of the A0 Lamb wave mode at cracks, AIP Conf. Proc. 1211, 129-136 (2010).
[28] P. Fromme, Influence of guided ultrasonic wave scattering directionality on the detection sensitivity for SHM of fatigue cracks, Proc. SPIE 7650, 76501M (2010). https://doi.org/10.1117/12.848621
[29] P. Fromme, Lamb wave (A0 mode) scattering directionality at defects, AIP Conf. Proc. 1806, 0300002 (2017). https://doi.org/10.1063/1.4974570
[30] J. Virieux, P-SV wave propagation in heterogeneous media: Velocity-stress finite-difference method, Geophysics 51, 889–901 (1986). https://doi.org/10.1190/1.1442147
[31] J.S. Hall and J.E. Michaels, Multipath ultrasonic guided wave imaging in complex structures, Struct. Health Moni. 14, 345–358 (2015). https://doi.org/10.1177/1475921715578316
[32] A. Ebrahimkhanlou, B. Dubuc, and S. Salamone, Damage localization in metallic plate structures using edge-reflected Lamb waves, Smart Mater. Struct. 25, 085035 (2016). https://doi.org/10.1088/0964-1726/25/8/085035